






Quantum typicality approach to energy flow between two spin-chain domains at different temperatures

Laurenz Beckemeyer ^{1,*} Markus Kraft ¹ Mariel Kempa ¹ Dirk Schuricht ² and Robin Steinigeweg ^{1,†}

¹*University of Osnabrück, Department of Mathematics/Computer Science/Physics, D-49076 Osnabrück, Germany*

²*Institute for Theoretical Physics, Utrecht University, 3584CC Utrecht, The Netherlands*

(Dated: August 1, 2025)

We discuss a quantum typicality approach to examine systems composed of two subsystems at different temperatures. While dynamical quantum typicality is usually used to simulate high-temperature dynamics, we also investigate low-temperature dynamics using the method. To test our method, we investigate the energy current between subsystems at different temperatures in various paradigmatic spin-1/2 chains, specifically the XX chain, the critical transverse-field Ising chain, and the XXZ chain. We compare our numerics to existing analytical results and find a convincing agreement for the energy current in the steady state for all considered models and temperatures.

I. INTRODUCTION

Over the last decades, the broad field of quantum many-body systems out of equilibrium has crystallized as one of the central topics of modern physics, both experimentally and theoretically [1–5], ranging from fundamental questions in statistical mechanics to applied questions in material science. The understanding of nonequilibrium physics has developed remarkably over the last years due to experimental advances [1], new theoretical concepts such as the typicality of pure states [6–30] and eigenstate thermalization [31–33], and the development of sophisticated numerical techniques [34–39].

One paradigmatic example of a nonequilibrium process is transport [40], a natural phenomenon in systems with one or more conserved quantities. Additionally, transport appears in both open and closed systems. In an open system scenario, transport processes are usually induced by coupling the system at its boundaries to external baths at different temperatures or chemical potentials. Then, in the long-time limit, a nonequilibrium steady state usually emerges with a characteristic density profile and a constant current [41–43]. Such a situation is often modeled by a quantum master equation of Lindblad form [44], which enables the application of sophisticated numerical techniques.

In a closed system scenario, a widely used approach for studying transport is linear response theory, where the Kubo formula in terms of autocorrelation functions plays a crucial role [45]. This theory predicts the behavior of a system near equilibrium, and it can be formulated either in frequency and momentum space or in the space and time domain. Another approach for studying transport in closed systems is a quantum quench [46–48]. Here, a quantum system is prepared in a particular initial state, typically an eigenstate of some pre-quench Hamiltonian. Then, the system undergoes a sudden change and is described by a new Hamiltonian, and the initial state

evolves unitarily according to this post-quench Hamiltonian. Quantum quenches can be studied in bipartite systems [49, 50], where the total system is composed of two subsystems and initially both subsystems are prepared in a state according to their respective Hamiltonians. Then, the subsystems are brought into contact together, and the total state evolves under the Hamiltonian of the total system.

Numerically, transport in open and closed systems has been investigated using various methods, including exact and Lanczos diagonalization [34, 35, 51], simulations based on matrix product states [38, 42, 52–56], and Monte-Carlo techniques [37, 39, 57, 58], to name a few. Additionally, the method of dynamical quantum typicality [26, 28] is a multifaceted method for investigating transport in closed quantum systems. The basic idea of dynamical quantum typicality is that one can imitate the expectation value of an entire ensemble by an expectation value of a single pure state, drawn at random from a high-dimensional Hilbert space. Dynamical quantum typicality has been used for linear-response functions, mostly at high temperatures [40]. For such temperatures, the statistical error is smaller than at low temperatures. Still, dynamical quantum typicality is a priori neither restricted to linear-response functions nor high temperatures.

In this work, we demonstrate the usefulness of dynamical quantum typicality in a specific physical situation, which differs from most previous applications in two ways. First, we apply it to energy flow in bipartite systems. Second, we also explore low temperatures. We do so for various spin-1/2 chains, which all feature ballistic energy transport: the XX chain, the critical transverse-field Ising chain, and the XXZ chain. We compare our numerical results to existing analytical results from conformal field theory (CFT) [50, 59] and generalized hydrodynamics (GHD) [49, 60, 61]. We find convincing agreement in all considered subsystem configurations of our bipartite setup, as well as for all examined temperatures. This agreement is not only found for the contact current but also for all local currents and densities in the steady state.

* lbeckemeyer@uos.de

† rsteinig@uos.de

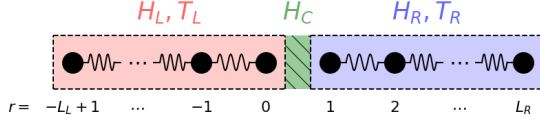


FIG. 1. Schematic representation of the setup. The total system consists of two subsystems described by H_L and H_R , respectively. Initially, they are prepared at temperatures T_L and T_R . The interaction of both parts for times $tJ \geq 0$ is described by the Hamiltonian H_C .

Our paper is structured as follows: In Sec. II, we define the bipartite setup used throughout the paper and the energy current between the two subsystems. After that, we introduce the different spin-1/2 chains in Sec. III, which we use for our subsystem configurations. Next, in Sec. IV, we discuss our quantum typicality approach to the energy current and briefly review the CFT results. Thereafter, we present our numerical results and compare them to analytical results in Sec. V. We conclude in Sec. VI and give directions for further research.

II. SETUP

Throughout our paper, we consider a system comprising two subsystems. Thus, the full Hamiltonian is written as

$$H = H_L + H_R + H_C, \quad (1)$$

where H_L and H_R are the Hamiltonian of the left subsystem and right subsystem, respectively. The term H_C describes the interaction between both subsystems. By L_L and L_R we denote the number of sites of the two subsystems such that $L = L_L + L_R$ is the total number of sites of the system. Here, we only focus on the equally sized case of $L_L = L_R = L/2$. A schematic representation of our setup is shown in Fig. 1.

In our paper, we are interested in the heat current from the left half into the right one. This heat current is given by [62]

$$Q_L = J_0 - \mu \dot{N}_L, \quad (2)$$

where $J_0 = -\dot{E}_L$ denotes the energy current flowing out of the left subsystem, \dot{N}_L is the particle current, and μ is a chemical potential. We focus on the case of $\mu = 0$. Thus, the heat current equals the energy current, $Q_L = J_0$. By using the Heisenberg equation of motion ($\hbar = 1$), we can express the energy current J_0 as

$$J_0 = -\dot{E}_L = -\frac{d}{dt} \langle H_L \rangle = i \langle [H_L, H] \rangle, \quad (3)$$

where the brackets denote the expectation value with respect to some state.

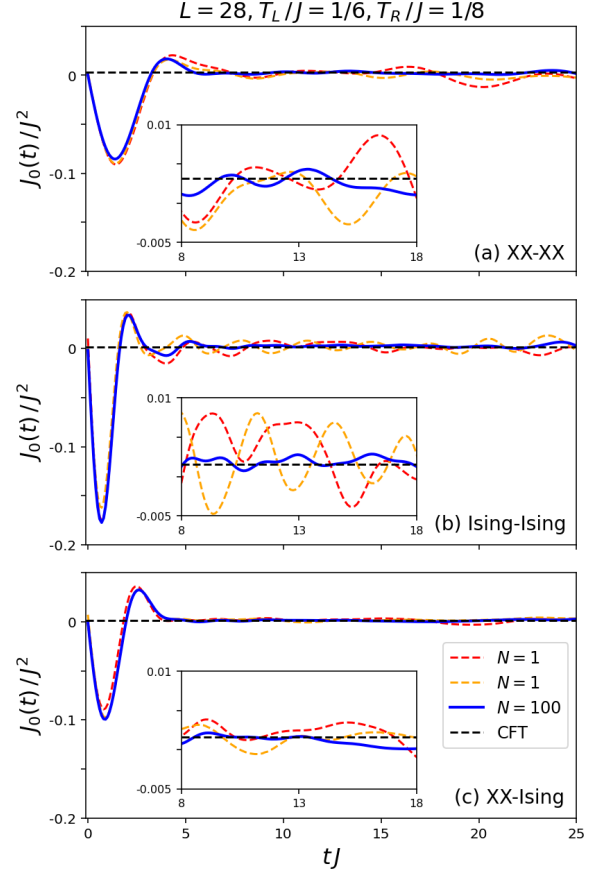


FIG. 2. Time evolution of the energy current for temperatures $T_L/J = 1/6, T_R/J = 1/8$, total system size $L = 28$ for the coupling of (a) two XX chains, (b) two critical Ising chains and (c) one XX chain to a critical Ising chain. Numerical data for two different pure random initial states ($N=1$) and for the average over many initial states ($N=100$) are compared to the CFT value.

Since we are interested in the energy current J_0 , we prepare both subsystems initially in a canonical ensemble with different low temperatures T_L and T_R with respect to the Hamiltonian H_L and H_R . Thus, we have the canonical states

$$\rho_{\beta_k} = \exp(-\beta_k H_k) / Z, \quad (4)$$

where $k = L, R$ denotes the subsystem, $\beta_k = 1/T_k$ the inverse temperature and $Z_k = \text{tr}[\exp(-\beta_k H_k)]$ the respective partition function. Here, we have set $k_B = 1$.

We investigate the energy current for various subsystem configurations, including the coupling of (i) two XX chains, (ii) two critical Ising chains, (iii) one XX chain to a critical Ising chain, and (iv) two XXZ chains. We introduce all models in the following.

III. MODELS

In our paper, we examine three different examples of spin-1/2 models, which correspond either to noninteracting systems or interacting integrable systems. All of them feature ballistic transport of energy. For simplicity, we focus on the homogeneous case and comment on the subsystem configuration afterwards. All models are one-dimensional lattice models of the type

$$H = \sum_{r=1}^{L-1} h_r, \quad (5)$$

where h_r are local Hamiltonians and L denotes again the number of lattice sites.

First, we introduce the spin-1/2 XXZ model. For this model, the local Hamiltonians are given by [40]

$$h_{\text{XXZ},r} = J (S_r^x S_{r+1}^x + S_r^y S_{r+1}^y + \Delta S_r^z S_{r+1}^z), \quad (6)$$

where S_r^i ($i = x, y, z$) are the spin-1/2 operators at site r , $J > 0$ is the antiferromagnetic exchange coupling constant, and Δ is the anisotropy in z direction. Using the Jordan-Wigner transformation [63], the spin-1/2 XXZ chain can be mapped onto a chain of spinless fermions. After this transformation, the local Hamiltonians in Eq. (6) take on the form

$$h_{\text{XXZ},r} = \frac{J}{2} (c_r^\dagger c_{r+1} + \text{h.c.}) + J\Delta \left(n_r - \frac{1}{2}\right) \left(n_{r+1} - \frac{1}{2}\right), \quad (7)$$

where c_r^\dagger and c_r are fermionic creation and annihilation operators at site r , and $n_r = c_r^\dagger c_r$ denotes the corresponding occupation number operator.

The second model we consider is the special case of the spin-1/2 XXZ chain with $\Delta = 0$, i.e., the XX chain. The local Hamiltonian reads

$$h_{\text{XX},r} = J (S_r^x S_{r+1}^x + S_r^y S_{r+1}^y). \quad (8)$$

This model is equivalent to a free-fermion chain, as can be seen by setting $\Delta = 0$ in Eq. (8) above.

The last spin model we investigate in this paper is the transverse-field Ising model. This model is described by the local Hamiltonian

$$h_{\text{Ising},r} = JS_r^x S_{r+1}^x + \frac{h}{2} (S_r^z + S_{r+1}^z), \quad (9)$$

where the constant h denotes the strength of the transverse magnetic field. Due to the Jordan-Wigner transformation, the transverse-field Ising model is, up to a constant, equivalent to the Kitaev chain [64–67],

$$h_{\text{Kitaev},r} = \frac{J}{4} (c_r^\dagger - c_r) (c_{r+1}^\dagger + c_{r+1}) + h n_r. \quad (10)$$

Throughout our paper, we focus on the critical transverse-field Ising chain. Therefore, we set $h = 1/2$.

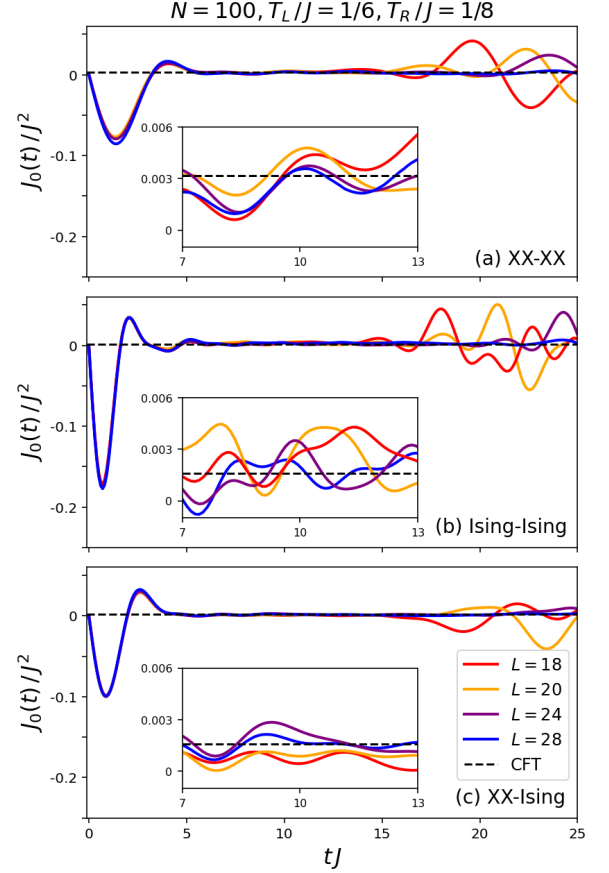


FIG. 3. Similar data as the one in Fig. 2 but now for different total system sizes L . Here, the numerical data are again averaged over $N = 100$ pure random initial states. For larger system sizes L , finite size effects are visible for later times tJ .

As mentioned earlier, we investigate total systems with L sites, composed of two subsystems with $L_L = L_R = L/2$ sites each. As indicated in Fig. 1, we slightly change notation and use for the left subsystem the sites $r = -L_L + 1, \dots, 0$ and for the right system the sites $r = 1, \dots, L_R$. The left subsystem interacts with the right subsystem at the sites $r = 0$ (left half) and $r = 1$ (right half). The interaction is described by the Hamiltonian H_C , which changes for our different configurations. We use in the case of (i) the coupling of two XX chains

$$H_C = J_C (S_0^x S_1^x + S_0^y S_1^y), \quad (11)$$

for the case of the coupling of (ii) two critical Ising chains and (iii) one XX chain to a critical Ising chain the term

$$H_C = J_C S_0^x S_1^x, \quad (12)$$

and for the coupling of (iv) two XXZ chains the term

$$H_C = J_C (S_0^x S_1^x + S_0^y S_1^y + \Delta C S_0^z S_1^z). \quad (13)$$

In our paper, we set $J_C = 1$ for all configurations. All chosen coupling Hamiltonians ensure that energy can

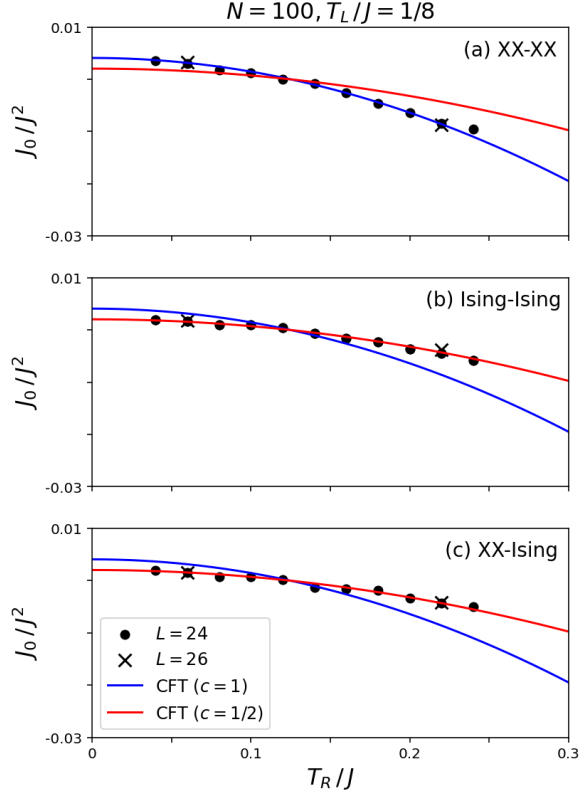


FIG. 4. Steady-state energy current J_0 versus temperature of the right subsystem T_R for the coupling of (a) two XX chains, (b) two critical Ising chains, and (c) one XX chain to a critical Ising chain for the total system size $L = 24$ and $T_L/J = 1/8$. The numerical data are compared to the CFT result (24).

flow between both subsystems. Before we proceed to our numerical results for the energy current in the various subsystem configurations, we introduce our dynamical typicality approach. We also briefly discuss the result obtained within CFT [59].

IV. METHODS

A. Dynamical typicality

We now turn to a discussion of dynamical quantum typicality (DQT) [26, 28], which is the key concept used in our numerical approach. We first focus on the homogeneous case of a single Hamiltonian H and a single temperature T , and afterwards come to the bipartite case with two H_L , H_R and two T_L , T_R .

The basic idea of DQT [10, 13, 14] is that one can approximate the expectation value of an ensemble density matrix,

$$\text{tr}[\rho(t)O], \quad \rho(t) = e^{-iHt} \rho e^{iHt}, \quad (14)$$

by an expectation value of just one pure state,

$$\langle \psi(t)|O|\psi(t) \rangle, \quad |\psi(t)\rangle = e^{-iHt} |\psi\rangle, \quad (15)$$

where O is a local operator. If ρ was the microcanonical ensemble and $|\psi\rangle$ an energy eigenstate, this idea would be identical to the well-known eigenstate thermalization hypothesis (ETH) [31–33]. In contrast to ETH, however, DQT is no assumption and relies on a particular construction of the pure state $|\psi\rangle$. Specifically, for a given ensemble density matrix ρ , this construction reads

$$|\psi\rangle = |\psi(0)\rangle \propto \sqrt{\rho} |\Phi\rangle, \quad (16)$$

which is the action of the square-root of ρ on a so-called Haar-random pure state $|\Phi\rangle$ [16]. This particular pure state $|\Phi\rangle$ does neither depend on ρ nor H . In an arbitrarily chosen orthogonal basis, it is given by

$$|\Phi\rangle \propto \sum_{m=1}^D c_m |m\rangle, \quad (17)$$

where D is the dimension of the Hilbert space and c_m are complex coefficients. Both, the real and imaginary part of these coefficients are drawn at random according to a Gaussian probability distribution with zero mean. For such a $|\Phi\rangle$ and the resulting $|\psi\rangle$, DQT then leads to the approximation [15, 16]

$$\text{tr}[\rho(t)O] = \frac{\langle \psi(t)|O|\psi(t) \rangle}{\langle \psi|\psi \rangle} + \varepsilon, \quad (18)$$

where the statistical error ε vanishes on average. More importantly, however, the standard deviation is bounded from above,

$$\sigma(\varepsilon) < b = \mathcal{O}\left(\frac{1}{\sqrt{D_{\text{eff}}}}\right). \quad (19)$$

Here, D_{eff} is the so-called effective dimension. In the case of the canonical ensemble $\rho \propto \exp(-\beta H)$, which is most relevant in the context of our work, the effective dimension is given by the partition function

$$D_{\text{eff}} = \text{tr}[\exp(-\beta(H - E_0))] \quad (20)$$

with the ground-state energy E_0 . Thus, D_{eff} counts the number of thermally occupied energy eigenstates. In the high-temperature limit $T \rightarrow \infty$, $D_{\text{eff}} = D = 2^L$ and hence the statistical error ε decreases exponentially fast with system size L . In the zero-temperature limit $T \rightarrow 0$, however, $D_{\text{eff}} = 1$ and thus the statistical error ε can be in principle large. Still, one has to take into account that the bound in Eq. (19) is not tight. In fact, at $T = 0$, it turns out that the statistical error becomes $\varepsilon = 0$. This fact is a kind of trivial consequence for a Haar-random pure state $|\Phi\rangle$: It is also random in the energy eigenbasis and the coefficient c_0 for the ground state $|0\rangle$ might be small but likely nonzero. At $T = 0$, only this coefficient survives and one has $|\psi\rangle = |0\rangle$ [68].

Let us next turn to the specific setup in Fig. 1, which is studied in our work. For this setup, we could proceed completely analogous and choose for the construction of

the pure state $|\psi\rangle$ in Eq. (16) an ensemble density matrix of the form

$$\rho \propto \exp(-\beta_L H_L) \otimes \exp(-\beta_R H_R). \quad (21)$$

While this choice is valid, the resulting $|\psi\rangle$ would be no product state of the two halves of the system, because $|\Phi\rangle$ is drawn at random from the full Hilbert space and thus highly entangled. Hence, to implement the product structure, we proceed slightly different and choose the pure state as

$$|\psi\rangle \propto \exp\left(-\frac{\beta_L H_L}{2}\right) |\Phi_L\rangle \otimes \exp\left(-\frac{\beta_R H_R}{2}\right) |\Phi_R\rangle, \quad (22)$$

where $|\Phi_L\rangle$ and $|\Phi_R\rangle$ are now drawn at random from the Hilbert space of the left and right half. While this choice does not change the typicality relation in Eq. (23), it goes along with a larger statistical error ε , which is given by the partition functions of the two halves, rather than the partition function of the entire system. To further reduce the statistical error, we average over $N = 100$ different realizations of $|\psi\rangle$,

$$\text{tr}[\rho(t)O] = \frac{1}{N} \sum_{i=1}^N \frac{\langle \psi_i(t) | O | \psi_i(t) \rangle}{\langle \psi_i | \psi_i \rangle}, \quad (23)$$

if not stated otherwise. In our case, the local observable O is mostly the contact current J_0 , but we also consider currents J_r at other sites r as well as the local energy densities h_r .

In our numerical simulations, we calculate the action of the imaginary-time operators $e^{-\beta_L H_L/2}$ and $e^{-\beta_R H_R/2}$ on the Haar-random pure states $|\Phi_L\rangle$ and $|\Phi_R\rangle$ with a fourth-order Runge-Kutta scheme, where we choose a very small step $\delta\beta J = 0.0001$. This scheme is also used for the action of the real-time operator e^{-iHt} on the pure state $|\psi\rangle$, where we choose a larger but still small step $\delta t J = 0.01$. By doing so and also using sparse-matrix techniques, we can treat system sizes outside the range of standard exact diagonalization. Alternatively, other propagation methods, such as Trotter decompositions [69–71] or Chebyshev polynomial expansions [72, 73], can be used as well.

B. Conformal field theory

The energy transport in a bipartite CFT setup has been studied by Bernard and Doyon [59]. Specifically they considered a CFT separated into two halves prepared at different temperatures. These halves were then glued together and the non-equilibrium steady state emerging at late times was studied. In particular, for the energy current they obtained the universal formula

$$J_E = \frac{\pi c}{12} (T_L^2 - T_R^2), \quad (24)$$

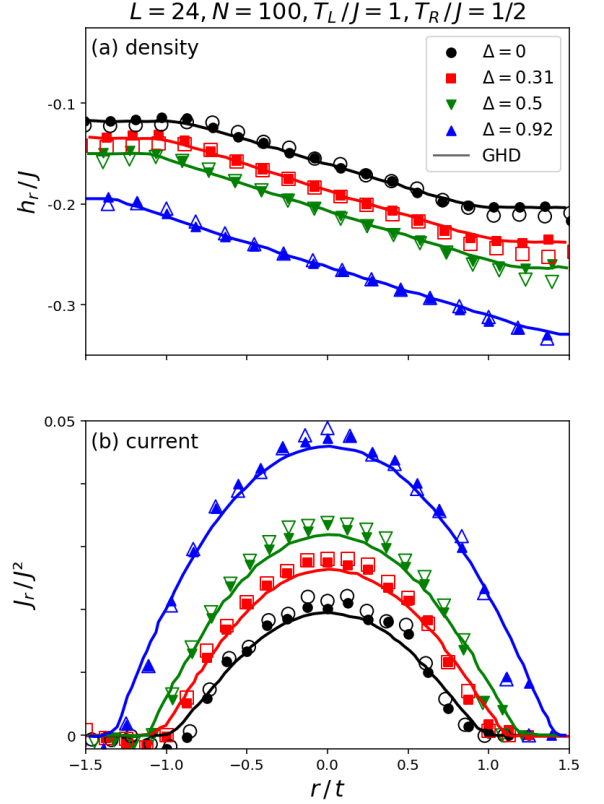


FIG. 5. Steady-state profile for (a) the local density $\langle h_r \rangle$ and (b) the local current $\langle J_r \rangle$ for the coupling of two XXZ chains with the same anisotropies Δ , $T_L/J = 1, T_R/J = 1/2$, and total system size $L = 24$. The numerical data are compared to the results from GHD in Ref. [49]. Here, the numerical data are shown for both, a random product state (open symbols) and a random state in the entire Hilbert space (closed symbols).

where c denotes the central charge of the CFT. Given that CFTs generically describe the universal low-energy behavior of certain lattice models, the result (24) is expected to hold only in the low-temperature regime. The central charge c is a specific characteristic of the CFT [74], physically it can be interpreted as the number of degrees of freedom, which here contribute to the energy transport through the system.

The setup leading to the universal CFT result (24) possesses translation invariance after the gluing quench. As an extension, Ref. [50] studied the coupling of an XX chain to a critical Ising chain, i.e., our setup (iii) above. Using both the non-equilibrium Green function formalism and the density matrix renormalization group method, the energy current was found to behave as

$$J_E = \frac{\pi}{12} \min(c_L, c_R) (T_L^2 - T_R^2). \quad (25)$$

This result can be viewed as a bottleneck effect, where the subsystem with the lower number of degrees of freedom as reflected by the lower central charge limits the energy

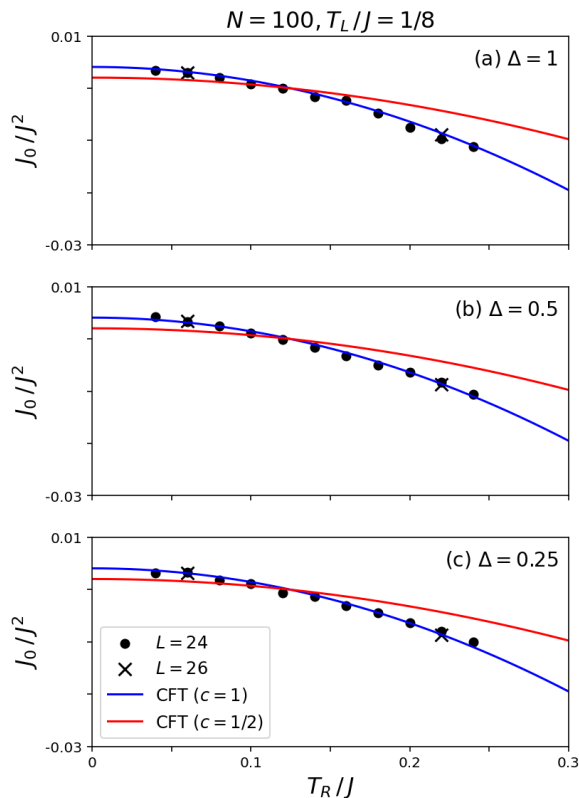


FIG. 6. Similar data as the one in Fig. 4 but now for the coupling of two XXZ chains with anisotropies (a) $\Delta = 1$, (b) $\Delta = 0.5$, and (c) $\Delta = 0.25$.

transport. The result (25) is also consistent with a purely field theoretic analysis by Bernard et al. [75], where, however, the precise link to a microscopic setup remains elusive.

V. RESULTS

Now, we turn to our numerical results, where we compare the energy current for various subsystem configurations to the value from CFT in Eq. (24). We first focus on the coupling of (i) two XX chains, (ii) two critical Ising chains, and (iii) one XX chain to a critical Ising chain. In CFT, the XX chain has the central charge $c = 1$ while the transverse-field Ising chain at the critical point has the central charge $c = 1/2$ [74].

To verify our numerical method initially, we compute the time evolution of the energy current J_0 for our considered subsystem configurations for systems with $L = 28$ sites and a fixed temperature of the left ($T_L/J = 1/6$) and right ($T_R/J = 1/8$) subsystem in Fig. 2. All subsystem configurations exhibit a transition regime characterized by oscillations and a buildup of correlations across the interface. After a specific timescale, the current reaches an approximately constant plateau, indicating the establishment of a non-equilibrium steady state.

Also in Fig. 2, we use two different realizations of a single random pure state and compare them with the average over $N = 100$ random pure states. With the averaging, the statistical error reduces remarkably, especially for the long-term behavior of the energy current J_0 . Furthermore, the steady state of the energy current agrees nicely with the value from CFT for all subsystem configurations. In the following, we average all our numerical results over $N = 100$ random pure initial states, if not stated differently.

Next, we investigate the dependence of the energy current on the total system size. We thus depict the time evolution of the energy current J_0 for varying total system sizes L and for the fixed initial temperatures of $T_L/J = 1/6$ and $T_R/J = 1/8$ in Fig. 3. For longer times, finite-size effects are visible for smaller L . Nevertheless, below the time where finite size effects are relevant, the data are close to the steady-state value according to CFT, especially for the coupling of an XX chain to the critical Ising chain, cf. Fig. 3 (c). In the following, we focus on total system sizes of $L = 24$, where finite-size effects and deviations from the CFT value are sufficiently small.

As one of our central results, we now calculate the steady-state energy current J_0 for a fixed initial temperature of $T_L/J = 1/8$ of the left subsystem and different initial temperatures of the right subsystem, see Fig. 4. We compare our numerics to the CFT values in Eq. (24) for $c = 1/2$ and $c = 1$. For all considered subsystem configurations (i) – (iii), we have a convincing agreement between our numerical results and CFT. Also our data do not significantly depend on system size, as we show in Fig. 4 by also calculating the energy current for exemplary temperatures T_R/J of the right subsystem for a total system size of $L = 26$. Furthermore, for the coupling of an XX chain to a critical Ising chain, the energy current is determined by the system with the lower central charge, which is, in this scenario, the critical Ising chain, see Fig. 4 (c). Consequently, we observe a bottleneck effect [50], where the energy transport is limited by the subsystem with the fewer degrees of freedom.

As the final subsystem configuration, we proceed to the (iv) coupling of two XXZ chains. We first focus on the case where all anisotropies are equal, i.e., $\Delta = \Delta_L = \Delta_R = \Delta_C$. We again benchmark our numerical calculation against existing results in the literature. In Fig. 5, we compare our numerics for a total system with $L = 24$ sites, fixed temperatures of the left and right subsystem, and different anisotropies Δ to results from GHD. The numerical data for the site dependence of the local energy density (Fig. 5 (a)) as well as the data for the site dependence of the local energy current (Fig. 5 (b)) matches the results of Ref. [49] convincingly. Here, the numerical data are shown for both, a random product state (open symbols) and a random state in the entire Hilbert space (closed symbols). As shown in Fig. 5, the statistical error for a random state in the entire Hilbert space is slightly smaller than the statistical error for a random product state.

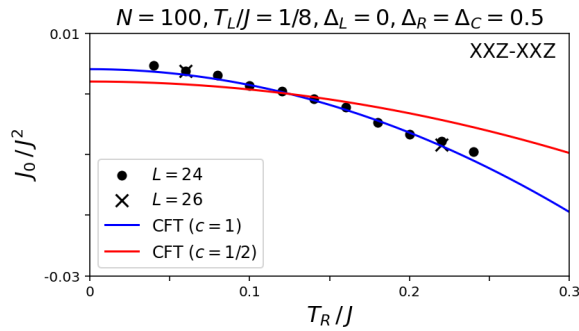


FIG. 7. Similar data as the one in Fig. 6 but now for the coupling of two XXZ chains with anisotropies $\Delta_L = 0$ and $\Delta_R = \Delta_C = 0.5$.

Focusing again on the contact site, we calculate the energy current J_0 for the coupling of two XXZ chains with total system size $L = 24$, fixed temperature $T_L/J = 1/8$, and the anisotropies $\Delta = 0.25, 0.5$, and 1.0 , see Fig. 6. For $-1 \leq \Delta < 1$, the ground state of the XXZ chain is gapless. The low-energy behavior of the XXZ chain in this regime is described by a CFT with central charge of $c = 1$ [76]. Again, we recover the temperature dependence in Eq. (24) for all considered anisotropies, and our data agrees with the CFT result convincingly and also do not significantly depend on system size.

At last, we also calculate the energy current J_0 for the coupling of two XXZ chains, but now with the anisotropies $\Delta_L = 0$ and $\Delta_R = \Delta_C = 0.5$. Additionally, in this case, we find convincing agreement with the CFT value, as shown in Fig. 7. Overall, this and the previous results demonstrate that our typicality approach is

suitable to capture the energy current down to low temperatures.

VI. CONCLUSION

To summarize, we discussed the method of dynamical quantum typicality, mostly used in linear response theory and at high temperatures, in less explored contexts. First, we applied it to energy flow between systems composed of two spin-chain domains at different temperatures and, second, to low temperatures. To test our method, we investigated the energy current in different spin-1/2 subsystem configurations, namely the coupling of (i) two XX chains, (ii) two critical Ising chains, (iii) one XX chain to a critical Ising chain, and (iv) two XXZ chains. We compared our numerical results to results from CFT and GHD. For all considered subsystem configurations and temperatures, we found a convincing agreement between our quantum typicality approach and these established methods. Therefore, we demonstrated the suitability of our approach for the study of bipartite systems at low temperatures. Further directions of research include additional models, such as the three-state quantum Potts chain, which in CFT has a central charge of $c = 4/5$.

ACKNOWLEDGMENTS

This work was funded by the Deutsche Forschungsgemeinschaft (DFG) under Grant No. 397067869 within the DFG Research Unit FOR 2692 under Grant No. 355031190.

-
- [1] I. Bloch, J. Dalibard, and W. Zwerger, *Many-body physics with ultracold gases*, *Rev. Mod. Phys.* **80**, 885 (2008).
 - [2] A. Polkovnikov, K. Sengupta, A. Silva, and M. Vengalattore, *Colloquium: Nonequilibrium dynamics of closed interacting quantum systems*, *Rev. Mod. Phys.* **83**, 863 (2011).
 - [3] J. Eisert, M. Friesdorf, and C. Gogolin, *Quantum many-body systems out of equilibrium*, *Nat. Phys.* **11**, 124 (2015).
 - [4] L. D'Alessio, Y. Kafri, A. Polkovnikov, and M. Rigol, *From quantum chaos and eigenstate thermalization to statistical mechanics and thermodynamics*, *Adv. Phys.* **65**, 239 (2016).
 - [5] D. A. Abanin, E. Altman, I. Bloch, and M. Serbyn, *Colloquium: Many-body localization, thermalization, and entanglement*, *Rev. Mod. Phys.* **91**, 021001 (2019).
 - [6] R. Alben, M. Blume, H. Krakauer, and L. Schwartz, *Exact results for a three-dimensional alloy with site diagonal disorder: Comparison with the coherent potential approximation*, *Phys. Rev. B* **12**, 4090 (1975).
 - [7] H. De Raedt and P. de Vries, *Simulation of two and three-dimensional disordered systems: Lifshitz tails and localization properties*, *Z. Phys. B* **77**, 243 (1989).
 - [8] J. Jaklič and P. Prelovšek, *Lanczos method for the calculation of finite-temperature quantities in correlated systems*, *Phys. Rev. B* **49**, 5065 (1994).
 - [9] A. Hams and H. De Raedt, *Fast algorithm for finding the eigenvalue distribution of very large matrices*, *Phys. Rev. E* **62**, 4365 (2000).
 - [10] J. Gemmer and G. Mahler, *Distribution of local entropy in the Hilbert space of bi-partite quantum systems: Origin of Jaynes' principle*, *Eur. Phys. J. B* **31**, 249 (2003).
 - [11] T. Iitaka and T. Ebisuzaki, *Algorithm for linear response functions at finite temperatures: Application to ESR spectrum of $s = \frac{1}{2}$ antiferromagnet Cu Benzoate*, *Phys. Rev. Lett.* **90**, 047203 (2003).
 - [12] J. Gemmer, M. Michel, and G. Mahler, *Quantum thermodynamics*, *Lect. Notes Phys.*, Vol. 657 (Springer, Berlin, 2004).
 - [13] S. Goldstein, J. L. Lebowitz, R. Tumulka, and N. Zanghì, *Canonical typicality*, *Phys. Rev. Lett.* **96**, 050403 (2006).

- [14] S. Popescu, A. J. Short, and A. Winter, *Entanglement and the foundations of statistical mechanics*, *Nat. Phys.* **2**, 754 (2006).
- [15] P. Reimann, *Typicality for generalized microcanonical ensembles*, *Phys. Rev. Lett.* **99**, 160404 (2007).
- [16] C. Bartsch and J. Gemmer, *Dynamical typicality of quantum expectation values*, *Phys. Rev. Lett.* **102**, 110403 (2009).
- [17] S. Sugiura and A. Shimizu, *Thermal pure quantum states at finite temperature*, *Phys. Rev. Lett.* **108**, 240401 (2012).
- [18] S. Sugiura and A. Shimizu, *Canonical thermal pure quantum state*, *Phys. Rev. Lett.* **111**, 010401 (2013).
- [19] T. A. Elsayed and B. V. Fine, *Regression relation for pure quantum states and its implications for efficient computing*, *Phys. Rev. Lett.* **110**, 070404 (2013).
- [20] R. Steinigeweg, J. Gemmer, and W. Brenig, *Spin-current autocorrelations from single pure-state propagation*, *Phys. Rev. Lett.* **112**, 120601 (2014).
- [21] T. Monnai and A. Sugita, *Typical pure states and nonequilibrium processes in quantum many-body systems*, *J. Phys. Soc. Jpn.* **83**, 094001 (2014).
- [22] H. Endo, C. Hotta, and A. Shimizu, *From linear to non-linear responses of thermal pure quantum states*, *Phys. Rev. Lett.* **121**, 220601 (2018).
- [23] J. Richter and R. Steinigeweg, *Combining dynamical quantum typicality and numerical linked cluster expansions*, *Phys. Rev. B* **99**, 094419 (2019).
- [24] A. Wietek, P. Corboz, S. Wessel, B. Normand, F. Mila, and A. Honecker, *Thermodynamic properties of the Shastry-Sutherland model throughout the dimer-product phase*, *Phys. Rev. Res.* **1**, 033038 (2019).
- [25] I. Rousochatzakis, S. Kourtis, J. Knolle, R. Moessner, and N. B. Perkins, *Quantum spin liquid at finite temperature: Proximate dynamics and persistent typicality*, *Phys. Rev. B* **100**, 045117 (2019).
- [26] T. Heitmann, J. Richter, D. Schubert, and R. Steinigeweg, *Selected applications of typicality to real-time dynamics of quantum many-body systems*, *Z. Naturforsch. A* **75**, 421 (2020).
- [27] J. Schnack, J. Richter, and R. Steinigeweg, *Accuracy of the finite-temperature lanczos method compared to simple typicality-based estimates*, *Phys. Rev. Res.* **2**, 013186 (2020).
- [28] F. Jin, D. Willsch, M. Willsch, H. Lagemann, K. Michielsen, and H. De Raedt, *Random state technology*, *J. Phys. Soc. Jpn.* **90**, 012001 (2021).
- [29] P. Reimann, *Dynamical typicality of isolated many-body quantum systems*, *Phys. Rev. E* **97**, 062129 (2018).
- [30] P. Mitrić, *Dynamical quantum typicality: Simple method for investigating transport properties applied to the Holstein model*, *Phys. Rev. B* **111**, 195140 (2025).
- [31] J. M. Deutsch, *Quantum statistical mechanics in a closed system*, *Phys. Rev. A* **43**, 2046 (1991).
- [32] M. Srednicki, *Chaos and quantum thermalization*, *Phys. Rev. E* **50**, 888 (1994).
- [33] M. Rigol, V. Dunjko, and M. Olshanii, *Thermalization and its mechanism for generic isolated quantum systems*, *Nature* **452**, 854 (2008).
- [34] J. Jaklič and P. Prelovšek, *Finite-temperature properties of doped antiferromagnets*, *Adv. Phys.* **49**, 1 (2000).
- [35] M. W. Long, P. Prelovšek, S. El Shawish, J. Karadamoglou, and X. Zotos, *Finite-temperature dynamical correlations using the microcanonical ensemble and the Lanczos algorithm*, *Phys. Rev. B* **68**, 235106 (2003).
- [36] U. Schollwöck, *The density-matrix renormalization group*, *Rev. Mod. Phys.* **77**, 259 (2005).
- [37] S. Grossjohann and W. Brenig, *Hydrodynamic limit for the spin dynamics of the Heisenberg chain from quantum Monte Carlo calculations*, *Phys. Rev. B* **81**, 012404 (2010).
- [38] U. Schollwöck, *The density-matrix renormalization group in the age of matrix product states*, *Ann. Phys. (NY)* **326**, 96 (2011).
- [39] H. De Raedt, F. Jin, M. I. Katsnelson, and K. Michielsen, *Relaxation, thermalization, and Markovian dynamics of two spins coupled to a spin bath*, *Phys. Rev. E* **96**, 053306 (2017).
- [40] B. Bertini, F. Heidrich-Meisner, C. Karrasch, T. Prosen, R. Steinigeweg, and M. Žnidarič, *Finite-temperature transport in one-dimensional quantum lattice models*, *Rev. Mod. Phys.* **93**, 025003 (2021).
- [41] M. Michel, M. Hartmann, J. Gemmer, and G. Mahler, *Fourier's Law confirmed for a class of small quantum systems*, *Eur. Phys. J. B* **34**, 325 (2003).
- [42] T. Prosen and M. Žnidarič, *Matrix product simulations of non-equilibrium steady states of quantum spin chains*, *J. Stat. Mech.* **2009**, P02035 (2009).
- [43] M. Žnidarič, *Spin transport in a one-dimensional anisotropic Heisenberg model*, *Phys. Rev. Lett.* **106**, 220601 (2011).
- [44] H.-P. Breuer and F. Petruccione, *The theory of open quantum systems* (Oxford University Press, Oxford, 2007).
- [45] R. Kubo, M. Toda, and N. Hashisume, *Statistical physics II: Nonequilibrium statistical mechanics*, Springer Series in Solid-State Sciences Vol. 31 (Springer, Berlin, 1991).
- [46] P. Calabrese and J. Cardy, *Time dependence of correlation functions following a quantum quench*, *Phys. Rev. Lett.* **96**, 136801 (2006).
- [47] A. Mitra, *Quantum quench dynamics*, *Annu. Rev. Condens. Matter Phys.* **9**, 245 (2018).
- [48] J. Richter, J. Herbrych, and R. Steinigeweg, *Sudden removal of a static force in a disordered system: Induced dynamics, thermalization, and transport*, *Phys. Rev. B* **98**, 134302 (2018).
- [49] B. Bertini, M. Collura, J. De Nardis, and M. Fagotti, *Transport in out-of-equilibrium XXZ chains: Exact profiles of charges and currents*, *Phys. Rev. Lett.* **117**, 207201 (2016).
- [50] S. Fischer, C. Karrasch, D. Schuricht, and L. Fritz, *Energy transport between critical one-dimensional systems with different central charges*, *Phys. Rev. B* **101**, 205146 (2020).
- [51] C. Karrasch, J. Hauschild, S. Langer, and F. Heidrich-Meisner, *Drude weight of the spin- $\frac{1}{2}$ XXZ chain: Density matrix renormalization group versus exact diagonalization*, *Phys. Rev. B* **87**, 245128 (2013).
- [52] G. Vidal, *Efficient simulation of one-dimensional quantum many-body systems*, *Phys. Rev. Lett.* **93**, 040502 (2004).
- [53] M. Zwolak and G. Vidal, *Mixed-state dynamics in one-dimensional quantum lattice systems: A time-dependent superoperator renormalization algorithm*, *Phys. Rev. Lett.* **93**, 207205 (2004).
- [54] F. Verstraete, V. Murg, and J. I. Cirac, *Matrix product states, projected entangled pair states, and varia-*

- tional renormalization group methods for quantum spin systems, *Adv. Phys.* **57**, 143 (2008).
- [55] H. Weimer, A. Kshetrimayum, and R. Orús, *Simulation methods for open quantum many-body systems*, *Rev. Mod. Phys.* **93**, 015008 (2021).
- [56] S. Paeckel, T. Köhler, A. Swoboda, S. R. Manmana, U. Schollwöck, and C. Hubig, *Time-evolution methods for matrix-product states*, *Ann. Phys. (NY)* **411**, 167998 (2019).
- [57] J. V. Alvarez and C. Gros, *Low-temperature transport in Heisenberg chains*, *Phys. Rev. Lett.* **88**, 077203 (2002).
- [58] M. Michel, O. Hess, H. Wichterich, and J. Gemmer, *Transport in open spin chains: A Monte Carlo wave-function approach*, *Phys. Rev. B* **77**, 104303 (2008).
- [59] D. Bernard and B. Doyon, *Energy flow in non-equilibrium conformal field theory*, *J. Phys. A: Math. Theor.* **45**, 362001 (2012).
- [60] O. A. Castro-Alvaredo, B. Doyon, and T. Yoshimura, *Emergent hydrodynamics in integrable quantum systems out of equilibrium*, *Phys. Rev. X* **6**, 041065 (2016).
- [61] B. Doyon, S. Gopalakrishnan, F. Möller, J. Schmiedmayer, and R. Vasseur, *Generalized hydrodynamics: A perspective*, *Phys. Rev. X* **15**, 010501 (2025).
- [62] F. Giazotto, T. T. Heikkilä, A. Luukanen, A. M. Savin, and J. P. Pekola, *Opportunities for mesoscopies in thermometry and refrigeration: Physics and applications*, *Rev. Mod. Phys.* **78**, 217 (2006).
- [63] P. Jordan and E. Wigner, *Über das paulische Äquivalenzverbot*, *Z. Physik* **47**, 631 (1928).
- [64] E. Lieb, T. Schultz, and D. Mattis, *Two soluble models of an antiferromagnetic chain*, *Ann. Phys.* **16**, 407 (1961).
- [65] P. Pfeuty, *The one-dimensional Ising model with a transverse field*, *Ann. Phys.* **57**, 79 (1970).
- [66] A. Y. Kitaev, *Unpaired Majorana fermions in quantum wires*, *Phys. Usp.* **44**, 131 (2001).
- [67] S. Suzuki, J. Inoue, and B. K. Chakrabarti, *Quantum Ising phases and transitions in transverse Ising models* (Springer, Berlin Heidelberg, 2013).
- [68] B. N. Balz, J. Richter, J. Gemmer, R. Steinigeweg, and P. Reimann, in *Thermodynamics in the Quantum Regime* (Springer, Cham, 2018) pp. 413–433.
- [69] M. Suzuki, *Decomposition formulas of exponential operators and Lie exponentials with some applications to quantum mechanics and statistical physics*, *J. Math. Phys.* **26**, 601 (1985).
- [70] H. De Raedt, *Product formula algorithms for solving the time dependent Schrödinger equation*, *Computer Physics Reports* **7**, 1 (1987).
- [71] D. W. Berry, G. Ahokas, R. Cleve, and B. C. Sanders, *Efficient quantum algorithms for simulating sparse Hamiltonians*, *Commun Math Phys* **270**, 359 (2006).
- [72] H. Tal-Ezer and R. Kosloff, *An accurate and efficient scheme for propagating the time dependent Schrödinger equation*, *J. Chem. Phys.* **81**, 3967 (1984).
- [73] A. Weiße, G. Wellein, A. Alvermann, and H. Fehske, *The kernel polynomial method*, *Rev. Mod. Phys.* **78**, 275 (2006).
- [74] P. Di Francesco, P. Mathieu, and D. Sénéchal, *Conformal field theory* (Springer, New York, 1997).
- [75] D. Bernard, B. Doyon, and J. Viti, *Non-equilibrium conformal field theories with impurities*, *J. Phys. A: Math. Theor.* **48**, 05FT01 (2015).
- [76] T. Giamarchi, *Quantum physics in one dimension* (Oxford University Press, Oxford, 2003).